Desalination and Water Treatment
www.deswater.com

doi: 10.5004/dwt.2020.26214

203 (2020) 58–69
November

Effect of $CaCl_2$ addition on crystal structure and separation performance of PVDF membranes: an experimental and molecular simulation study

Yue Song[a], Jiacong Li[a], Guorong Xu[b], Ming Zhang[a,*], Hai Xin[a], Zihan Liu[a], Xintao Zuo[a], Wenyuan Fan[a]

[a]*School of Chemistry and Chemical Engineering, Tianjin Key Laboratory of Organic Solar Cells and Photochemical Conversion, Tianjin University of Technology, Tianjin 300384, China, Tel. +86 22 6021 4259; emails: zm2404@tjut.edu.cn (M. Zhang), 15822763588@163.com (Y. Song), ljc9433@163.com (J. Li), xin13821765171@163.com (H. Xin), lzhan424@163.com (Z. Liu), xintaozuo@126.com(X. Zuo), wyfan@tjut.edu.cn (W. Fan)*

[b]*The Institute of Seawater Desalination and Multipurpose Utilization, Ministry of Nature Resources (MNR), Tianjin 300192, China, Tel. +86 22 8789 6336; email: laxgr@aliyun.com (G. Xu)*

Received 4 November 2019; Accepted 6 June 2020

ABSTRACT

The inorganic salts addition can affect the interactions among the polymer chains and further influence the membrane structure. In this work, the effects of calcium chloride ($CaCl_2$) on the crystal structure and separation performance of poly(vinylidene fluoride) (PVDF) membranes were studied. The influence of $CaCl_2$ addition with varying concentrations (0–3 wt.%) was investigated by X-ray diffraction (XRD), Fourier transform infrared spectroscopy (FTIR), scanning electron microscopy (SEM), and molecular dynamic (MD) simulations. XRD and FTIR characterizations indicated that $CaCl_2$ could induce the transformation of PVDF crystal structure from α to β, which was further confirmed by molecular dynamic simulation. The MD simulation results revealed that the interaction between Ca^{2+} and F atom distorted the dihedral angle of PVDF chains, inducing the crystal structure transforming partially. SEM characterization indicated that the finger-like voids became longer and broader with increasing amount of $CaCl_2$ addition. The membrane consisting of 0.7 wt.% $CaCl_2$ exhibited the best performance with bovine serum solution rejection of 84.7% and water permeability of 203.6 L m^{-2} h^{-1} bar^{-1}.

Keywords: Calcium chloride; PVDF membrane; Crystal form transform; Molecular dynamic simulation; Mechanism

1. Introduction

Considering the irreplaceable role of clean water in promoting the sustainable development of economy [1], the problem of water pollution induced by the rapid development of industrialization has become increasingly prominent. Traditional methods, such as evaporation, flocculation, activated-sludge, are faced with great challenge in meeting the strict requires of environment because of disadvantages of high operating cost, huge cover area, and long duration. Owing to the obvious advantages such as high separation efficiency, low cost, and high operation flexibility, membrane technology has become a superior separation method and played a vital role in separation processes in recent years. Due to the high mechanical strength, thermal stability, and chemical resistance, poly(vinylidene fluoride) (PVDF) has been evidenced to be an excellent alternative materials in membrane separation [2], and PVDF

* Corresponding author.

membranes have been extensively applied in water and wastewater treatment, chemical industry, medicine, food, and other fields [3,4]. However, the main problem of PVDF membrane focuses on membrane fouling and contamination by proteins, other impurities and/or microorganism in water due to its hydrophobic nature, which leads to an enormous decrease of permeability.

In recent years, various efforts, such as physical blending [5], chemical grafting [6], and surface modifications [7], have been devoted to improve the anti-fouling and separation performance of PVDF membrane. Typically, addition of inorganic salts in casting dope during phase inversion process is one of the effective practice to improve the permeability and/or rejection of PVDF membranes [8]. Lithium chloride (LiCl), which has excellent solubility in both water and various organic solvents, has attracted much attention as a pore forming additive in the preparation of PVDF membranes [9]. For example, Park et al. [10] added LiCl to the polymer dope solution to form a sponge-like structure with reduced macrovoid. Tomaszewska [11] found that increasing LiCl addition could lead to the formation of larger cavities and result in the increase of porosity, but the mechanical strength was drastically reduced.

In order to obtain the high-performance membrane, other inorganic salts were employed as additives. Kim et al. [12] reported that the addition of zinc chloride ($ZnCl_2$) on membrane formation could lead to higher rejection but lower water permeability. Idris et al. [13] reported that the membrane with 2 wt.% lithium bromide (LiBr) exhibited excellent separation activity and the pure water flux recovery up to 90%. Noor et al. [8] reported that the addition of sodium bromide (NaBr) could endow the membrane with certain negative charge, which could prevent the aggregation of particles on membrane surface and improve their antifouling capability. However, all the above studies focused on the relationship between the dose of additive and the separation performance of the membrane.

As a matter of fact, PVDF is a semi-crystalline polymer [14,15], polymer crystallinity and crystal phase also play an important role in determining mechanical strength and separation performance of the membranes [16–18]. In Nawi et al. [17], they found the dope solution temperature could affect the transformation of α- to β-phase, and the membrane with more β-phase exhibited better flux. However, Li et al. [18] research indicated that the solvent of PVDF dope did not affect the crystallinity of PVDF.

Recently, Sun et al. [19] revealed that the addition of SiO_2 could induce the partial crystal phase transformation of PVDF from α to β phase, which was attributed to the hydrogen bond between SiO_2 and PVDF polymer chain. Lin et al. [20] studied the lithium perchlorate ($LiClO_4$) addition on the morphology and crystal structure of PVDF membranes by wet phase inversion process. They also found that the PVDF crystallites became into β form at the high salt dopes (e.g., >5 wt.%). However, the mechanism of the inorganic salts impact on PVDF crystal form is still not clear.

In the past years, the lithium halogenated-based additives and their effects on membrane properties and performance have been widely explored and reported [21]. Compared with lithium salts, inorganic additive of calcium chloride is cheaper and easy to obtain. However, there are few reports of addition of $CaCl_2$ on the separation performance especially on the crystal structure of PVDF membrane.

From this point of view, our work herein aimed to systematically study the influence of inorganic salt additive of $CaCl_2$ on crystal structure and performance of PVDF membranes. Particularly, the mechanism for the crystal transformation induced by the interaction of the inorganic salt and polymer was revealed by molecular simulation (MD). The results obtained here can both shed light on designing high-performance PVDF membrane and promoting application of polymer membrane.

2. Experimental

2.1. Chemicals

PVDF (761A molecular weight: 7×10^5 g mol^{-1}) was purchased from Arkema, France. Poly(vinyl pyrrolidone) (PVP) (molecular weight: 58,000, K29–32), calcium chloride anhydrous ($CaCl_2$, AR, >96%) and N,N-dimethylacetamide (DMAc, reagent grade) were supplied by Fuchen Chemical Reagents Co., (Tianjin). Bovine serum albumin (BSA) (molecular weight: 68,000 Da) was obtained from Yuanye Biological Co., (Shanghai). Deionized water was prepared using a Simplicity® UV system and used for all tests. All chemicals were used as received without further purification.

2.2. Membrane preparation

The PVDF membranes were prepared by the phase inversion method. Firstly, the $CaCl_2$ salts were dispersed in DMAc and sonicated for 0.5 h. Then the PVDF and PVP were added in the above mixture and it was stirred at 60°C for 6 h to obtain casting solution. In order to remove suspended gas-bubbles from the solution, the resulting homogenous casting solution was kept at 60°C for 12 h in a vacuum oven before casting. The dope solution was poured onto a clean glass plate at room temperature and it was casted on a glass plate using a casting knife with approximately 200 μm gate height. The glass plate with the thin membrane was then immersed into a deionized water bath without any delay to remove the residual DMAc and the additives. The dope solutions prepared consist of 17 wt.% PVDF and various compositions of $CaCl_2$ and PVP are given in Table 1.

2.3. Membrane characterization

2.3.1. X-ray diffraction

X-ray diffraction (XRD) patterns of the as-prepared samples were collected on a Rigaku Ultima IV diffractometer with Cu Kα radiation (λ = 0.15406 nm). Data were recorded in a 2θ range from 5° to 80° with a step size of 0.01°, and the step interval is 2 s.

2.3.2. Fourier transform infrared spectroscopy

The crystalline phase or phases present in each sample were measured and collected using Fourier transform infrared spectroscopy (FTIR, STA6000-TL9000-MS, USA).

Table 1
Dope solution formulation of PVDF membranes

Membrane	PVDF (wt.%)	$CaCl_2$ (wt.%)	PVP (wt.%)	DMAc (wt.%)
M0	17.0	0.0	0.0	83.0
M1	17.0	0.0	1.0	82.0
M2	17.0	0.5	1.0	81.5
M3	17.0	0.7	1.0	81.3
M4	17.0	0.9	1.0	81.1
M5	17.0	1.0	1.0	81.0
M6	17.0	2.0	1.0	80.0
M7	17.0	3.0	1.0	79.0

The spectra were recorded in a wave number range of 4,000–600 cm^{-1} by cumulating 64 scans at a resolution of 2 cm^{-1}.

2.3.3. Scanning electron microscopy

Scanning electron microscopy (SEM, ZEISS-MERLIN-Compact, Germany) was used to examine the morphology of the PVDF membranes by the standard methods. The membrane samples were snapped in liquid nitrogen so as to give a generally clean break. Then the samples were dried in a vacuum oven and coated by sputtering platinum to ensure excellent conductivity prior to analysis.

2.3.4. Conductivity

The conductivity of water bath was tested using a conductivity meter (DDSJ-308A, China) to analyze the diffusion of the $CaCl_2$ salts from the solid phase (membrane) to the liquid phase (water bath). The results were shown in supporting information.

2.3.5. Contact angle

The contact angle was tested by a contact angle analyzer (SCA20, Germany). Sample coupons were prepared by cutting pieces at random locations within the membrane sheets. The sample was placed on a glass plate (top side up) and fixed with tape. Then, a drop of distilled water (5 μL) was placed on the surface using a micro-syringe. The contact angle was measured at five different locations for each membrane sample so as to ensure reproducibility of data.

2.3.6. Porosity

Based on the results of the gravimetric method, the overall porosity of the membranes (ε) was calculated through Eq. (1) [22]:

$$\varepsilon = \frac{\left(W_{wet} - W_{dry}\right) / \rho_{H_2O}}{S \times L} \quad (1)$$

where W_{wet} and W_{dry} are the weight of the wet and dry membrane, g, respectively, S is the membrane effective area, cm^2, L is the membrane thickness, cm and ρ_{H_2O} is the density of water g mL^{-1}.

2.4. Membrane evaluation

The water permeability and BSA rejection of membranes were evaluated using dead-end filtration system (shown in Fig. 1), which was consisted with a nitrogen cylinder, an Amicon 8200 filtration cell (Millipore, 200 mL), a magnetic stirrer (Corning, PC-420D) and an electronic balance (Adventure pro, AV8101).

The membranes were tested for water permeation fluxes using deionized water at 0.2 MPa. The water permeate flux (J) and permeability (k) of the membranes were obtained by using the following equations:

$$J = \frac{V}{S \times \Delta t} \quad (2)$$

$$k = \frac{J}{p} \quad (3)$$

where V is the volume of the solution, L, S is the effective area of the ultrafiltration membrane, m^2, Δt is the filtration time, h, and p is the transmembrane pressure, bar.

The rejection rates of the membranes were determined by separation experiments using BSA solutions with concentration of 1.0 g L^{-1} at a pressure of 0.2 MPa.

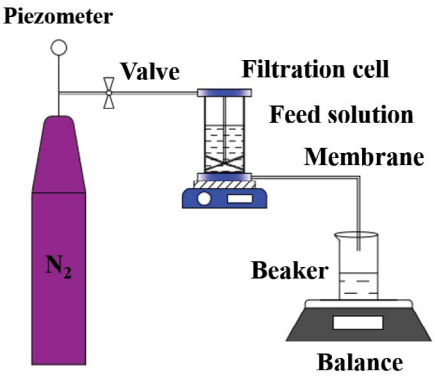

Fig. 1. Experimental apparatus of membrane performance test.

The concentration of BSA in the feed and permeate solutions was measured by using UV-vis spectrometer (HACH DR6000, USA) at wavelength of 280 nm. The solute rejection of membrane was calculated using Eq. (4):

$$R = \frac{C_0 - C_t}{C_0} \times 100 \quad (4)$$

where R is the rejection rate of BSA, %, C_0 and C_t are BSA concentration in feed solution and permeate solution, respectively, mol L^{-1}.

2.5. Antifouling property evaluation

The antifouling property of membrane was evaluated by BSA solution of 1.0 g L^{-1}. First, the membrane was pre-pressured at 0.2 MPa with deionized water for 20 min in the dead-end filtration set up system until the flux reached a stable value and recorded the water flux J_{W1} (L m^{-2} h^{-1}). Subsequently, BSA solution replaced the deionized water at a testing pressure of 0.2 MPa for 20 min, and then the membrane was taken out. To remove the foulant from the surface, the membrane was immersed into deionized water for 20 min and then were rinsed with cool tap water without sponge or hand contact. The cell was also washed and recharged by deionized water, then the membrane was reloaded and tested again by deionized water, the water flux of cleaned membranes J_{W2} (L m^{-2} h^{-1}) was tested and recorded.

In order to examine the antifouling property clearly, the flux recovery rate (FRR) was defined and calculated by Eq. (5):

$$\mathrm{FRR} = \frac{J_{W2}}{J_{W1}} \times 100\% \quad (5)$$

2.6. Molecular simulation methods

In order to understand the interaction of $CaCl_2$ with the PVDF and the transformation of PVDF crystalline phase, the molecular dynamic (MD) simulations were carried out using Materials Studio software [23]. The models of PVDF shown in Fig. 2 with various ratio (consistent with experiments) were constructed using the Amorphous Cell module, which is part of the Materials Studio suite of programs. The model is a cube of 30.5 × 30.5 × 30.5 $Å^3$, including 24 α crystal form PVDF chains, and each chain consists of 20 CH_2–CF_2 monomer units [24]. The number of PVDF chains and $CaCl_2$ in each structure and the total number of atoms in each case were shown in Table 2.

The COMPASS force field [25] was used in this work. Firstly, the system was relaxed by the geometry optimization, the box was adjusted to a size with a density around 1.78 g cm^{-3}. Secondly, the system was subjected to annealing cycles of 2 ns duration wherein the temperature was increased linearly from 300 to 1,000 K with a time step size of 1 fs in the NPT ensemble at 1 atm. After annealing, the system was cooled to 300 K in 2 ns time intervals [26]. Finally, the MD simulation at 300 K and 1 atm was performed for an additional 1,000 ps with a time step of 1 fs to reach the equilibrium condition and remove residual stress. Snap shots of the system were saved every 1,000 steps and the last 200 snap shots were used for further analysis of the structures.

3. Results and discussion

3.1. Effect of $CaCl_2$ addition on the crystal form of PVDF membranes

In order to study the effect of $CaCl_2$ addition on crystal structures of PVDF membrane, XRD measurement was carried out and the result is shown in Fig. 3. The peaks at

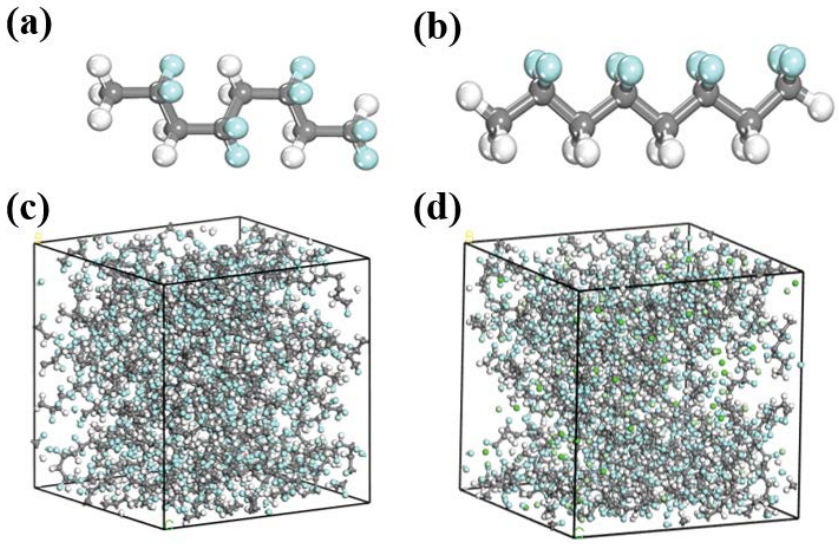

Fig. 2. Simulation model of the PVDF membrane. (a) Crystallize structure of α-PVDF segment, (b) crystallize structure of β-PVDF segment, (c) PVDF model without $CaCl_2$, and (d) PVDF model with $CaCl_2$. The gray-white balls represent H atoms, the gray-black balls represent C atoms, the blue balls represent F atoms, the green balls represent Ca^{2+} ion, and the light green balls represent Cl^- atoms.

Table 2
Model information of MD simulations

$CaCl_2$ weight fraction (%)	Number of PVDF chains	Number of $CaCl_2$	Total atom numbers
0	24	0	2,928
0.5	24	8	2,952
0.7	24	12	2,964
0.9	24	15	2,973
1.0	24	17	2,979
2.0	24	32	3,024
3.0	24	48	3,072

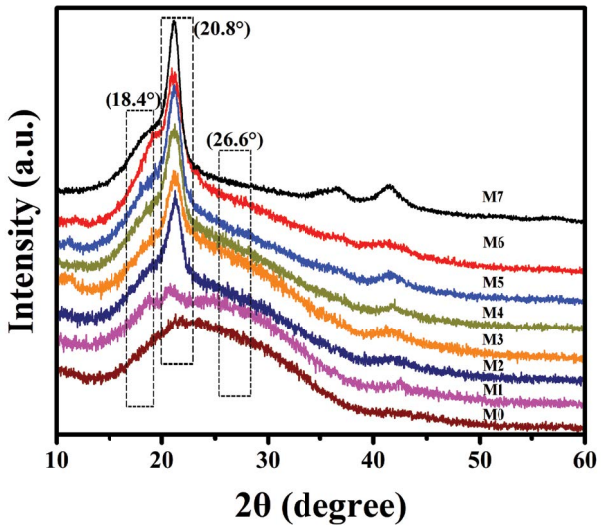

Fig. 3. XRD patterns of PVDF membranes with and without PVP and/or $CaCl_2$ addition.

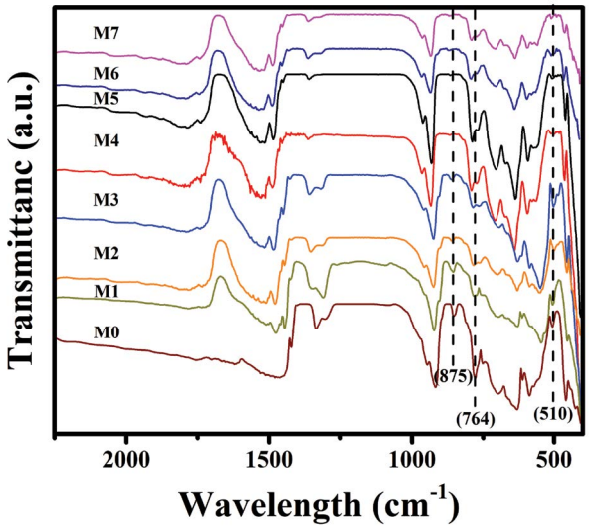

Fig. 4. FTIR spectra of membranes with and without PVP and/or $CaCl_2$ addition.

2θ = 18.46°, 20.24°, and 26.68° are attributed to the diffractions of (200), (110), and (201) planes of α crystal in PVDF, and the peak at 2θ = 20.8° is attributed to the diffraction of (110) plane of β crystal in PVDF [27,28]. For the pure PVDF membrane (M0 in Fig. 3), the big peak in the range of 18°–26° indicates its amorphous structure. However, PVDF membrane with 1 wt.% PVP doping shows two obvious peaks at 2θ = 18.4° and 20.8°, which are ascribed to (200) plane of α and (110) plane of β crystal form, indicating the mixed crystal structure of α and β. Furthermore, weakening of the peak at 2θ = 18.4° and strengthening of the peak at 2θ = 20.8° after $CaCl_2$ addition indicate the formation of more β-phase. Intriguingly, this phenomenon is consistent with the results of lithium salt addition in PVDF membrane [20], in which the β-phase was enhanced with the increased amount of $LiClO_4$. In order to reveal the mechanism of $CaCl_2$ impact on the PVDF crystal form, molecular simulations were further carried out in section 3.2 (Interaction between $CaCl_2$ and PVDF).

For the better identification of the crystal phases, infrared spectroscopy was performed for all fabricated samples (shown in Fig. 4). It was reported that, the α crystal of PVDF exhibits a transgauche (TGTG′; shown in Fig. 2a) conformation with characteristic absorption bands at 764, 875, and 976 cm^{-1} [29], while the β crystal of PVDF exhibits an all trans (TTTT; shown in Fig. 2b) conformation with characteristic absorption bands at 510 cm^{-1} [30]. From FTIR spectrum, it can be noted that the increase of $CaCl_2$ addition obviously weakens the absorption peaks at 764 and 875 cm^{-1} (corresponding to α crystal form) while enhances the peak at 510 cm^{-1} (corresponding to β crystal form), indicating the conversion of PVDF crystal from α to β. This is consistent with the XRD results.

3.2. Interaction between $CaCl_2$ and PVDF

As mentioned above, the difference between PVDF α and β crystal forms was caused by the configuration of C–C–C–C skeleton. For the α-PVDF (shown in Fig. 2a), the sequential four dihedral angles formed by the backbone carbon atoms arrange in the trans-gauche-trans-gauche′ (TGTG′) conformation, whose dihedral angles are 180° (T) and 60° (G). For the β crystal form (shown in Fig. 2b), the dihedral angles are formed by backbone carbon atoms which are in the trans (TTTT) conformation, and the dihedral angles all correspond to 180°. Accordingly, a higher fraction of local trans configuration indicates a higher fraction of β crystal form in the membrane.

Fig. 5 shows the distributions of dihedral angles for backbone C–C–C–C of PVDF chain with various $CaCl_2$ addition after 1 ns MD simulation. It can be seen that there are two major peaks at 60° and 170° for all cases, in which the peak at 60° only corresponds to α crystal form and the peak at 170° corresponds to both α and β crystal form. For the case without $CaCl_2$, the peak at 60° was higher and the peak at 170° was lower. With the increase of $CaCl_2$ additive, the peak at 60° is weakened and the peak at 170° is strengthened. This result indicated that the $CaCl_2$ addition can convert part of the α crystal form to the β crystal form. Furthermore, for the case of 0.7 wt.% $CaCl_2$, the peak at 170° is higher than other ratios, which means that the ratio of β crystal form in the PVDF membrane is the highest. This simulation results are consistent with our XRD and FTIR results.

In order to identify the interaction between $CaCl_2$ and PVDF chains, the radial distribution function (RDF) were analyzed. RDF is commonly used to characterize extended molecular structure. The RDF represents the probability of finding a pair of atoms at a distance *r* with respect to the bulk in a completely random distribution. The Ca^{2+}–F RDF results of different membranes with various $CaCl_2$ addition were analyzed (shown in Fig. 6a). The obvious peaks among 1.8–2.5 Å indicated that interaction between Ca^{2+} of $CaCl_2$ and F atom of PVDF chain. When the addition of $CaCl_2$ was 0.7 wt.%, the sharp peak of Ca^{2+}–F means strongest binding between Ca^{2+} and F atom. Fig. 6b shows the RDF of the intra-molecular Ca^{2+} and Cl^- of $CaCl_2$ with H and F of PVDF in the membrane with 0.7 wt.% $CaCl_2$ addition. It can be found that the intra-molecular Ca^{2+}–F RDF peak was higher than the Ca^{2+}–H, Cl^-–H, and Cl^-–F RDF peaks, which can be contributed to the stronger interactions of Ca^{2+} and F compared with that of other atom pairs. The typical conformation of PVDF chain with the exist of $CaCl_2$ is shown in the top left corner of Fig. 6b. The distances between Ca^{2+} and F atoms in PVDF are as close as 2.1 Å, indicating the Ca^{2+} strongly interacts with PVDF via Ca^{2+}–F binding. Thus,

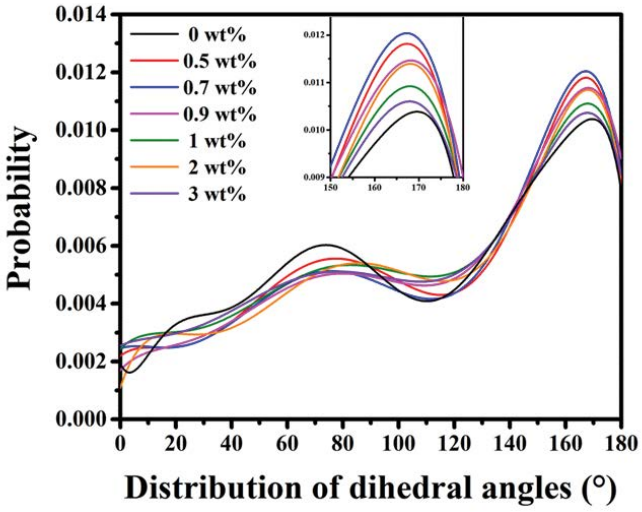

Fig. 5. Distribution of backbone C–C–C–C dihedral angles of the PVDF membranes with 0, 0.5, 0.7, 0.9, 1, 2, and 3 wt.% $CaCl_2$ addition.

the stronger binding induces the carbon backbone of PVDF chain to exhibit the zigzag conformation, which was in accordance with β crystal form. Recently, Theng et al. [31] studied the interaction of PVDF with ionic liquid adopting molecular dynamic simulation, and they also found that PVDF has a stronger interaction with $[C2bim]^+$ cation.

3.3. Morphology characterization of membranes

The cross-sectional SEM images of all the fabricated PVDF membranes with different $CaCl_2$ additions are shown in Fig. 7. All the membranes demonstrate the asymmetric morphology characterized by a thin skin and a porous bulk. The morphology of pure PVDF membrane exhibits a hamburger structure (Fig. 7a), in which the upper and bottom

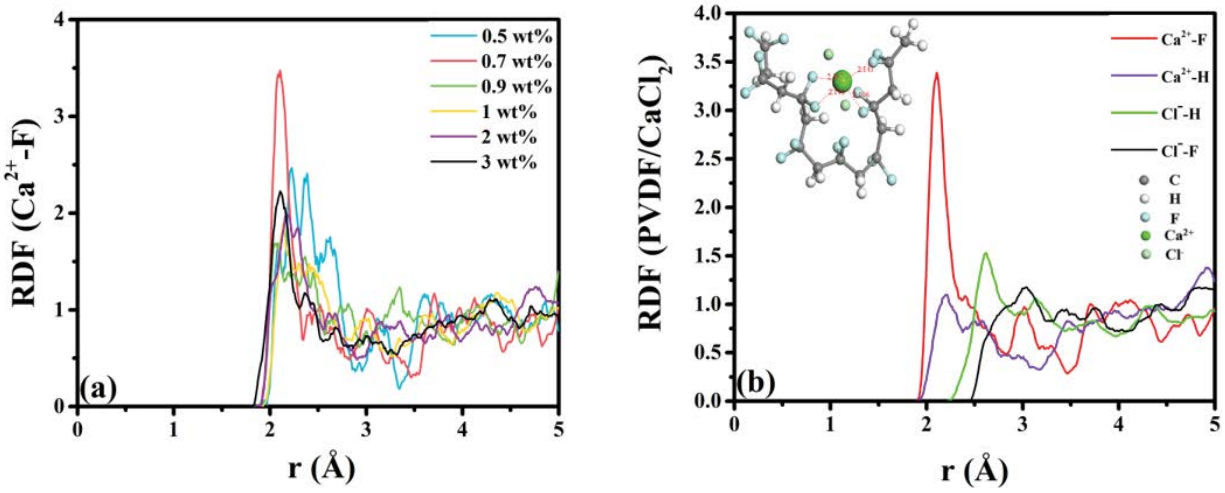

Fig. 6. Radial distribution functions: (a) the Ca^{2+}-F of the membranes with 0.5, 0.7, 0.9, 1, 2, and 3 wt.% $CaCl_2$ addition and (b) $Ca^{2+}$and Cl^- of $CaCl_2$ with H and F of PVDF for the membrane of 0.7 wt.% $CaCl_2$ addition and a typical conformation of PVDF chain at top left corner.

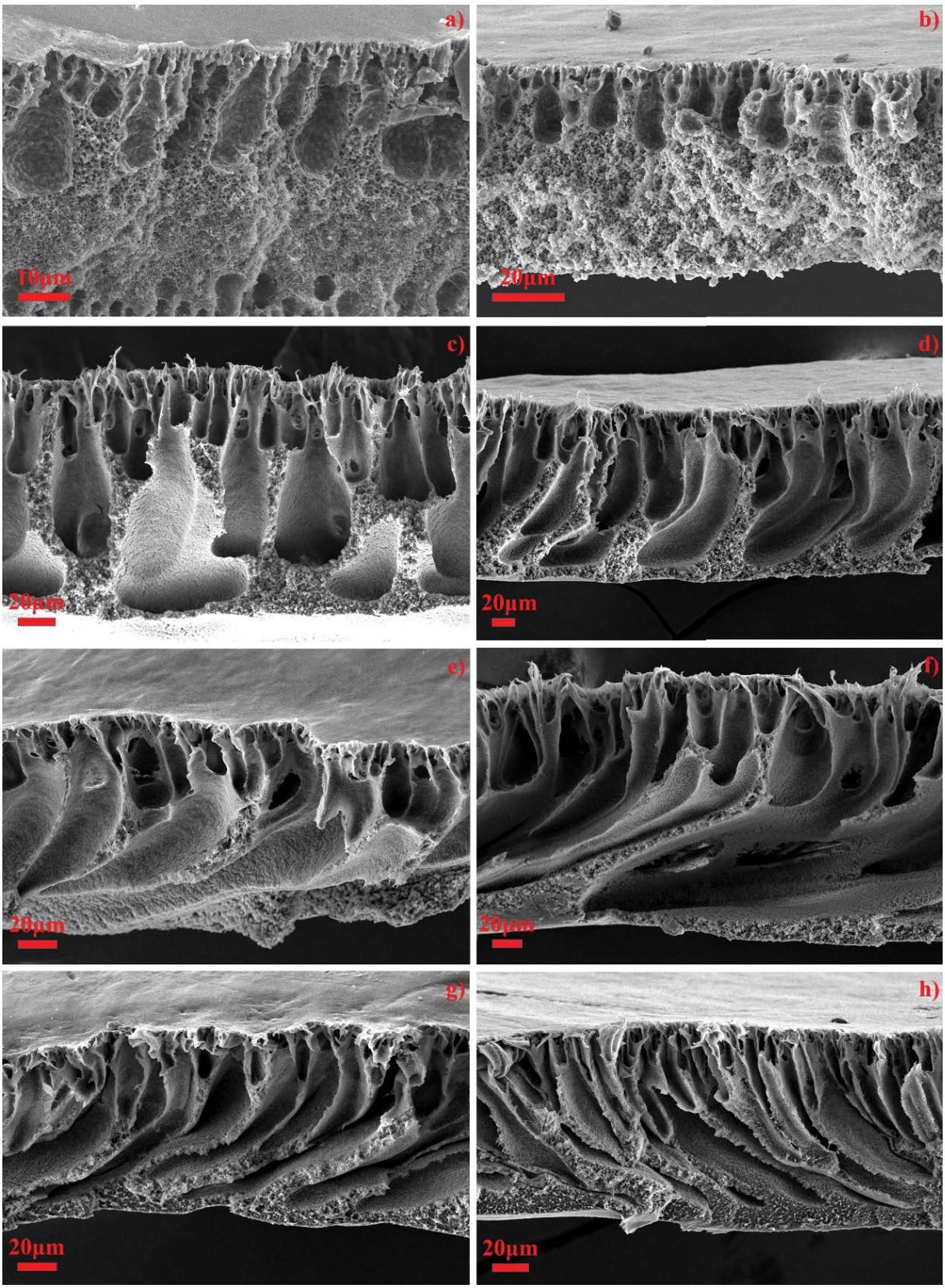

Fig. 7. Cross-section SEM images for PVDF membranes with and without PVP and/or $CaCl_2$ addition: (a) pure PVDF, (b) 1 wt.% PVP, (c) 1 wt.% PVP and 0.5 wt.% $CaCl_2$, (d) 1 wt.% PVP and 0.7 wt.% $CaCl_2$, (e) 1 wt.% PVP and 0.9 wt.% $CaCl_2$, (f) 1 wt.% PVP and 1 wt.% $CaCl_2$, (g) 1 wt.% PVP and 2 wt.% $CaCl_2$, and (h) 1 wt.% PVP and 3 wt.% $CaCl_2$.

layers provide a finger-like structure and the middle layer shows a compact cellular pore structure. Due to the existence of continuously cellular pores, permeability of pure PVDF membrane is very low. Addition of 1 wt.% PVP endows PVDF membrane with irregular large voids (Fig. 7b), which can be ascribed to the enhancement of liquid–liquid demixing process during precipitation of the dope solution since PVP is miscible with water [32].

Addition of $CaCl_2$ in the casting solutions induces great changes for the fabricated PVDF membranes (Figs. 7c–h). Compared with the irregular macrovoids formed in membrane with PVP addition, $CaCl_2$ additive induces the formation of the regular finger-voids with some small cellular pores between finger voids. In addition, the finger voids become more elongated and regular with increasing amount of $CaCl_2$ (Figs. 7c–e). The formation of regular finger voids in membrane with $CaCl_2$ (Figs. 7c–e) can be attributed to the interaction between the calcium and PVDF chains. As mentioned in Fig. 6, the cation of Ca^{2+} can enhance the interaction among the PVDF chains by the Ca^{2+}–F binding in the casting dope.

Generally, the properties of casting solution can affect the liquid–liquid demixing process. In the phase separation process, salt tends to go into the liquid micelle rather than stay in the concentrated gel phase that contains a great number of polymer. For the system of $CaCl_2$ and PVDF, the liquid micelle with some dissolve calcium salt is formed from liquid–liquid demixing. Since the cell wall may act somewhat like a skin layer, a large osmosis force is created between the micelle and the surrounding gel phase. This force drives the non-solvent of water into the micelle, which further accelerates the growth of macrovoids. Such phenomena has also been observed by Strathmann [32] in early years. The increase of calcium salt ratio promotes the formation of spongy-like membrane structure interrupted by macrovoids, which can enhance the formation of pores and improve the pore interconnectivity. As shown in Table 3, when the content of $CaCl_2$ was more than 1 wt.%, larger pores are formed without any distinct change in porosity.

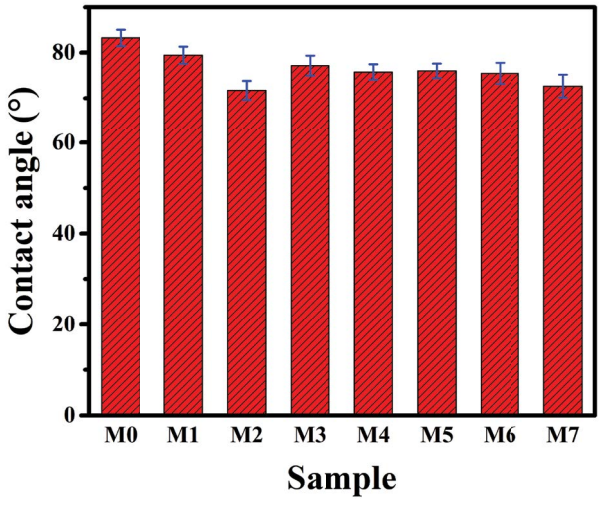

Fig. 8. Contact angle values of various PVDF membranes.

3.4. Hydrophilicity

The surface hydrophilicity, which is generally evaluated by water contact angle, can affect the permeability and anti-fouling ability of membrane. The hydrophilicity of every membrane is analyzed and the results are shown in Fig. 8. Addition of $CaCl_2$ induces the contact angel decrease from 79° to 73°, indicating the hydrophilicity is slightly enhanced.

3.5. Separation and anti-fouling performance of PVDF membrane with $CaCl_2$ addition

Fig. 9 shows the pure water permeability of the PVDF membrane without $CaCl_2$ addition and those with different ratio of $CaCl_2$ combined with PVP. For the membrane (M0) without $CaCl_2$ and PVP, the permeability is only 10 L m^{-2} h^{-1} bar^{-1}. But the permeability of M1 with 1 wt.% PVP increases to 80 L m^{-2} h^{-1} bar^{-1}. Furthermore, the membranes (M2–M7) with additive of PVP and $CaCl_2$ show obvious increase in both permeability and rejection rates. When the $CaCl_2$ content is 0.7 wt.%, the permeability of the membrane is 203.6 L m^{-2} h^{-1} bar^{-1} (M3). With increase of $CaCl_2$ content to 1.0 wt.% (M5), the water flux almost keeps stable. But further increasing $CaCl_2$ amount to 3 wt.% (M7), the water flux decreases to 125 L m^{-2} h^{-1} bar^{-1}. At the same time, the membranes with $CaCl_2$ showed higher

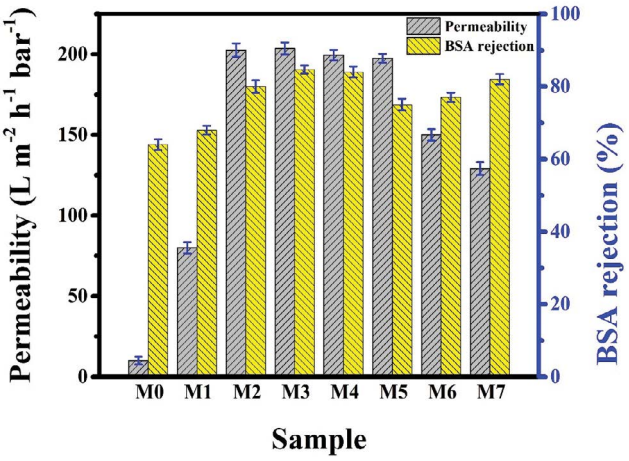

Fig. 9. Permeability and the BSA rejection rate of membranes.

Table 3
Porosity of PVDF membranes with various $CaCl_2$

Membrane	Porosity (%)
M0	66.3
M1	81.2
M2	78.1
M3	79.6
M4	81.5
M5	86.4
M6	80.5
M7	76.5

rejection rates compared with the membrane (M0, M1) without $CaCl_2$ addition, M3 membrane approximately has rejection of 84.7%. However, membranes (M0, M1) without $CaCl_2$ additive have lower rejection rate around 70%. Results show that the M3 membrane exhibits both higher flux and high rejection rates, indicating the addition of 0.7% $CaCl_2$ tends to create more and small pores, which improved not only the permeation rate but also the rejection rate. But, the membranes with higher $CaCl_2$ additive amounting of 2 wt.% (M6) and 3 wt.% (M7) have lower permeability, which can be contributed to crystallization of high concentration $CaCl_2$ in the voids of membrane [33]. This results also do consist with the SEM figures of voids for various $CaCl_2$ addition (shown in Fig. 7).

In order to further investigate the anti-fouling performance of the membrane, the FRRs of membranes with and without $CaCl_2$ were tested. As shown in Fig. 10, the FFR of the PVDF membrane without $CaCl_2$ was only 46.6%. However, with increasing the amount of $CaCl_2$, the value of FFR gradually increases. The pure water flux recovery of PVDF membrane with 2 wt.% $CaCl_2$ is as high as 98.8%. The increase in the pure water flux recovery of $CaCl_2$ addition might be ascribed to the weakened interaction between the membrane surface and the contaminants, which is induced by the change in the crystal form of the membrane. The increased antifouling capability could facilitate the cleaning of the contaminants in the membrane operations.

4. Conclusion

In conclusion, our study indicates that the presence of $CaCl_2$ displays a significant effect on the crystal structure and separation performance of PVDF membranes. The addition of $CaCl_2$ not only induces the formation of the β crystal phase in the PVDF membrane, but also improves the pore structure and the performance x of the membrane. The molecular dynamic simulation reveals that the strong binding between Ca^{2+} and F atom helps the PVDF chain transform from α to β crystal structure. The addition of 0.7 wt.% $CaCl_2$ is sufficient to induce the interaction between the inorganic salts and the polymer chains in the casting solution. $CaCl_2$ leads to the formation of the regular finger-voids, which is beneficial for the membrane separation performance. The fabricated PVDF membranes with $CaCl_2$ additions show an obvious increase in both water flux and BSA rejection. The PVDF membrane with 2 wt.% $CaCl_2$ addition shows greatest anti-fouling performance, in which the membrane flux recovery reaches 98.8%. This investigation not only develops a promising and cheaper inorganic salt additive for PVDF membrane, but also provides a better understanding about the effects of small additive on the crystal form and separation performance of polymer membrane.

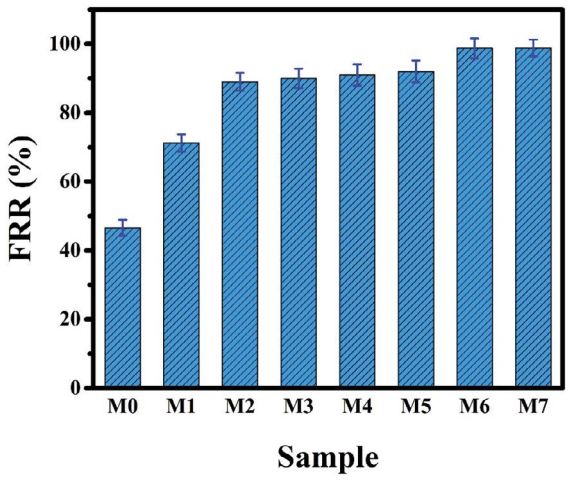

Fig. 10. Flux recovery rate (FRR) of membranes with $CaCl_2$.

Acknowledgments

This research was funded by a grant of Tianjin Enterprise Science and Technology Commissioner Project [18JCTPJC48600], Tianjin Natural Science Foundation [16JCYBJC19400], and Training Project of Innovation Team of Colleges and Universities in Tianjin [TD13–5020]. We also acknowledge National Supercomputing Center in Shenzhen for providing the computational resources and Materials Studio 7.0.

References

[1] X.L. Qu, P.J.J. Alvarez, Q.L. Li, Applications of nanotechnology in water and wastewater treatment, Water Res., 47 (2013) 3931–3946.
[2] F. Liu, N.A. Hashim, Y. Liu, M.R.M. Abed, K. Li, Progress in the production and modification of PVDF membranes, J. Macromol. Sci., 375 (2011) 1–27.
[3] N.P. Khumalo, L.N. Nthunya, E. De Canck, S. Derese, A.R. Verliefde, A.T. Kuvarega, B.B. Mamba, S.D. Mhlanga, D.S. Dlamini, Congo red dye removal by direct membrane distillation using PVDF/PTFE membrane, Sep. Purif. Technol., 211 (2019) 578–586.
[4] C.A. Quist-Jensen, F. Macedonio, E. Drioli, Membrane crystallization for salts recovery from brine—an experimental and theoretical analysis, Desal. Water Treat., 57 (2015) 7593–7603.
[5] B. Yang, X. Yang, B. Liu, Z. Chen, C. Chen, S. Liang, L.-Y. Chu, J. Crittenden, PVDF blended PVDF-g-PMAA pH-responsive membrane: effect of additives and solvents on membrane properties and performance, J. Macromol. Sci., 541 (2017) 558–566.
[6] Y. Yang, J. Chen, Y. Li, D. Shi, B. Lin, S. Zhang, Y. Tang, F. He, K. Lam, Preparation and dielectric properties of composites based on PVDF and PVDF-grafted graphene obtained from electrospinning-hot pressing method, J. Macromol. Sci., Part A Pure Appl. Chem., 55 (2017) 148–153.
[7] Z. Anari, A. Sengupta, K. Sardari, S.R. Wickramasinghe, Surface modification of PVDF membranes for treating produced waters by direct contact membrane distillation, Sep. Purif. Technol., 224 (2019) 388–396.
[8] N.D.M. Noor, N.M. Yusof, I. Ahmed, M. Hesampour, A. Idris, Influence of sodium bromide additive on polyethersulfone, J. Appl. Polym. Sci., 128 (2012) 1–10.
[9] F. Mokhtari, M. Latifi, M. Shamshirsaz, M. Khelghatdoost, S. Rahmani, Modeling of electrospun PVDF/LiCl nanogenerator by the energy approach method: determining piezoelectric constant, J. Text. Inst., 108 (2017) 1917–1925.
[10] S.-H. Park, Y. Ahn, M. Jang, H.-J. Kim, K.Y. Cho, S.S. Hwang, J.-H. Lee, K.-Y. Baek, Effects of methacrylate based amphiphilic block copolymer additives on ultra filtration PVDF membrane formation, Sep. Purif. Technol., 202 (2018) 34–44.
[11] M. Tomaszewska, Preparation and properties of flat-sheet membranes from poly(vinylidene fluoride) for membrane distillation, Desalination, 104 (2003) 1–11.

[12] S.R. Kim, K.H. Lee, M.S. Jhon, The effect of $ZnCl_2$ on the formation of polysulfone membrane, J. Membr. Sci., 119 (1996) 59–64.
[13] A. Idris, I. Ahmed, M.A. Limin, Influence of lithium chloride, lithium bromide and lithium fluoride additives on performance of polyethersulfone membranes and its application in the treatment of palm oil mill effluent, Desalination, 250 (2010) 805–809.
[14] H.-H. Chang, S.-C. Chen, D.-J. Lin, L.-P. Cheng, The effect of Tween-20 additive on the morphology and performance of PVDF membranes, J. Membr. Sci., 466 (2014) 302–312.
[15] R. Thomas, E. Guillen-Burrieza, H.A. Arafat, Pore structure control of PVDF membranes using a 2-stage coagulation bath phase inversion process for application in membrane distillation (MD), J. Membr. Sci., 452 (2014) 470–480.
[16] M.G. Buonomenna, P. Macchi, M. Davoli, E. Drioli, Poly(vinylidene fluoride) membranes by phase inversion: the role the casting and coagulation conditions play in their morphology, crystalline structure and properties, Eur. Polym. J., 43 (2007) 1557–1572.
[17] N.I.M. Nawi, M.R. Bilad, N.A.H.M. Nordin, M.O. Mavukkandy, Z.A. Putra, M.D.H. Wirzal, J. Jaafar, A.L. Khan, Exploiting the interplay between liquid-liquid demixing and crystallization of the PVDF membrane for membrane distillation, Int. J. Polym. Sci., 2018 (2018) 1–10.
[18] Y. Li, C. Jin, Y. Peng, Q. An, Z. Chen, J. Zhang, L. Ge, S. Wang, Fabrication of PVDF hollow fiber membranes via integrated phase separation for membrane distillation, J. Taiwan Inst. Chem. Eng., 95 (2019) 487–494.
[19] H. Sun, Y. Liu, D. Li, B. Liu, J. Yao, Hydrophobic SiO_2 nanoparticle-induced polyvinylidene fluoride crystal phase inversion to enhance permeability of thin film composite membrane, J. Appl. Polym. Sci., 136 (2019) 1–12, doi: 10.1002/app.48204.
[20] D.-J. Lin, C.-L. Chang, F.-M. Huang, L.-P. Cheng, Effect of salt additive on the formation of microporous poly(vinylidene fluoride) membranes by phase inversion from $LiClO_4$/water/DMF/PVDF system, Polymer, 44 (2003) 413–422.
[21] R.J. Sengwa, P. Dhatarwal, Predominantly chain segmental relaxation dependent ionic conductivity of multiphase semi-crystalline PVDF/PEO/$LiClO_4$ solid polymer electrolytes, Electrochim. Acta, 338 (2020) 1–20.
[22] S. Ayyaru, Y.-H. Ahn, Application of sulfonic acid group functionalized graphene oxide to improve hydrophilicity, permeability, and antifouling of PVDF nanocomposite ultrafiltration membranes, J. Membr. Sci., 525 (2017) 210–219.
[23] Accelrys Software Inc., Materials Studio Release Notes, Release 7.0, Accelrys Software Inc., San Diego, 2013.
[24] T. Hu, B. Hu, Y. Yan, The predicted dielectric constant of an amorphous PVDF changing with temperature by molecular dynamics simulations, Int. J. Electrochem. Sci., 13 (2018) 10088–10100.
[25] H. Sun, P. Ren, J.R. Fried, The COMPASS Forcefield: parameterization and validation for polyphosphazenes, Comput. Theor. Polym. Sci., 8 (1998) 229–246.
[26] H.-L. Chen, S.-P. Ju, C.-Y. Lin, C.-T. Pan, Investigation of microstructure and mechanical properties of polyvinylidene fluoride/carbon nanotube composites after electric field polarization: a molecular dynamics study, Comput. Mater. Sci., 149 (2018) 217–229.
[27] R. Gregorio, Determination of the α, β, and γ crystalline phases of poly(vinylidene fluoride) films prepared at different conditions, J. Polym. Sci., 100 (2006) 3272–3279.
[28] D.M. Esterly, B.J. Love, Phase transformation to β-poly (vinylidene fluoride) by milling, J. Polym. Sci., 42 (2004) 91–97.
[29] K.J. Kim, J.C. Yong, Y.H. Kim, Factors determining the formation of the β crystalline phase of poly(vinylidene fluoride) in poly(vinylidene fluoride)-poly(methyl methacrylate) blends, Vib. Spectrosc., 9 (1995) 147–159.
[30] V. Sencadas, R. Gregorio, S. Lanceros-Méndez, α to β phase transformation and microestructural changes of PVDF films induced by uniaxial stretch, J. Macromol. Sci. Part B Phys., 48 (2009) 514–525.
[31] S.G. Theng, K.B. Jumbri, M.D.H. Wirzal, Molecular Dynamics Simulation of Membrane in Room Temperature Ionic Liquids, AIP Conference Proceedings, AIP Publishing LLC, 2017.
[32] H. Strathmann, Production of microporous media by phase inversion processes, ACS Symp. Ser., 269 (1985) 165–195.
[33] M.A. Kraus, M. Nemas, M.A. Frommer, The effect of low molecular weight additives on the properties of aromatic polyamide membranes, J. Appl. Polym. Sci., 23 (2010) 445–452.

Supplementary information

S1. Existing form of $CaCl_2$ in the membrane

Inorganic particles play a significant role in formation and regulation of structure and properties of PVDF membranes. We monitored the conductivity of water bath. As shown in Fig. S1, when the glass plate was immersed into the pure water bath, the conductivity increased rapidly from 1.5 to 18.6 μS cm^{-1} in few minutes, and then the conductivity remained the same, which indicated that the leaching of Ca^{2+} has achieved a balance in the water. After the fresh water was replaced into the bath, the conductivity kept stably with a low value of 1.5 μS cm^{-1}, which was as same as pure water. This result indicated that Ca^{2+} diffused quickly from the solid phase into the liquid phase during the process of phase inversion. Due to the big solubility of $CaCl_2$ in water, it can be considered that few of Ca^{2+} existed in the PVDF membrane. The calcium salt only plays a role of regulating pore structures and induces crystal form of the PVDF membrane.

In order to identify whether the Ca^{2+} existed in the PVDF membrane, the energy dispersive spectrometer (EDS) of PVDF membrane was also tested. As shown in Fig. S2, it can be found there were no peaks of element calcium and chlorine, which indicated that there was almost no residue of $CaCl_2$ in the PVDF membrane. It was well-consistent with the conductivity test results.

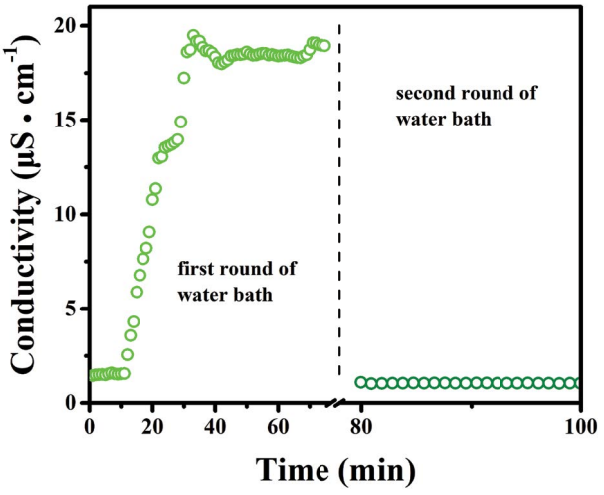

Fig. S1. Conductivity change in a gel bath of membrane (M5).

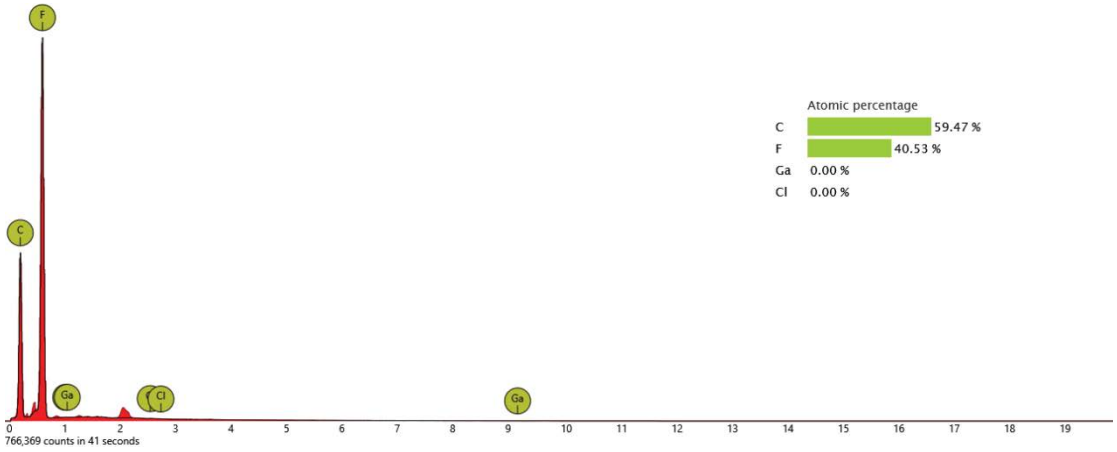

Fig. S2. Energy dispersive spectrometer(EDS) analysis of cross-section for PVDF membrane.

S2. Separation and anti-fouling performance of PVDF membrane with addition of LiCl, $CaCl_2$, and $FeCl_3$

The separation and anti-fouling performance of membranes with different inorganic salts were tested. As shown in Fig. S3, the water permeability of membrane with addition of $CaCl_2$ is higher than the other membranes with LiCl and $FeCl_3$. Furthermore, the flux recovery rate of membrane with $CaCl_2$ is as high as 98.8%, which is also better than the other two membranes with LiCl and $FeCl_3$. However, the BSA rejection of membrane with LiCl exhibits a little higher than the two membranes with addition of $CaCL_2$ and $FeCl_3$. The difference can be contributed to the interaction between the inorganic salts and PVDF chains, which also could provide various pore distribution in the membrane.

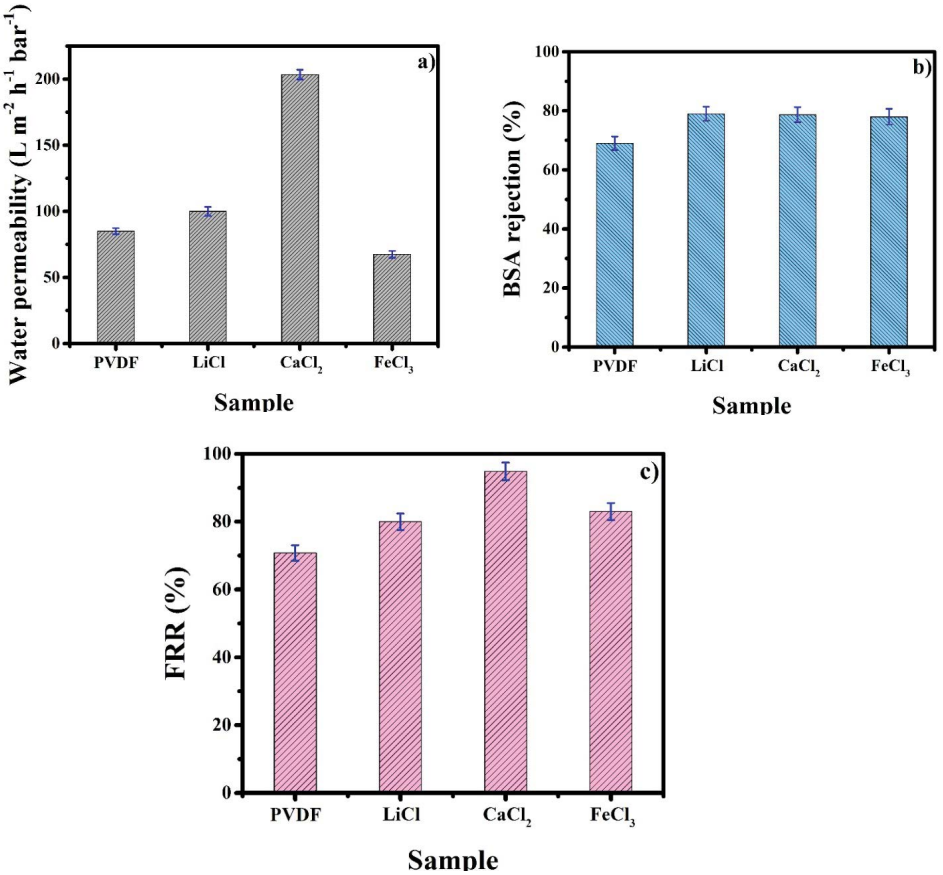

Fig. S3. Performance of PVDF membrane with different inorganic salt: (a) pure water flux, (b) BSA rejection, and (c) flux recovery rate (FRR).

S3. Pore distribution of PVDF membrane with addition of $CaCl_2$

As shown in Fig. S4, the small size pores were found on the surface of PVDF membrane with 1 wt.% $CaCl_2$ addition. This evidence further supported the conclusion that the water permeability of membrane with addition of $CaCl_2$ is higher than that of the membranes with LiCl and $FeCl_3$ addition.

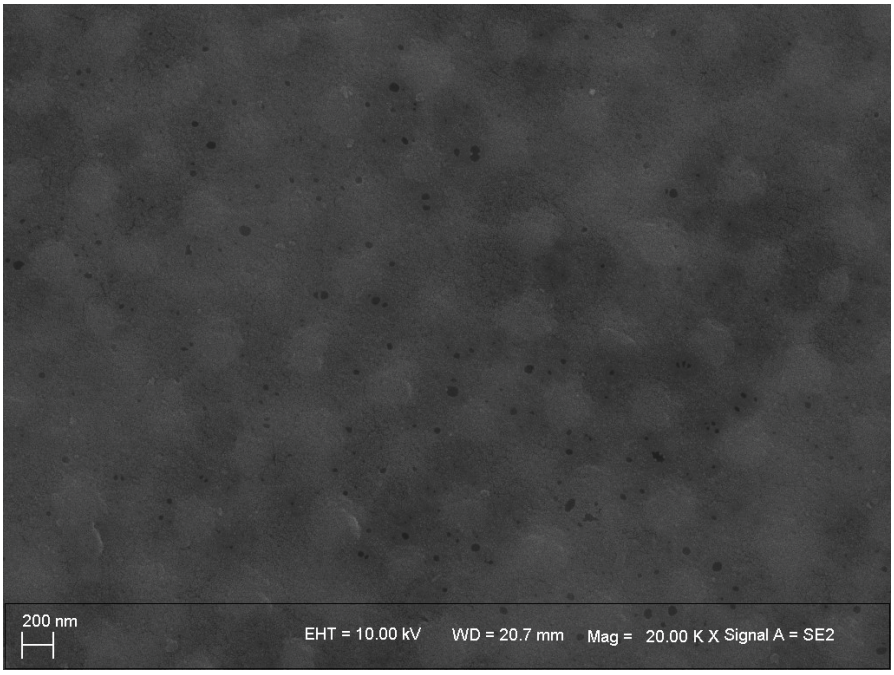

Fig. S4. SEM image of surface structure of membrane with 1 wt.% CaCl2 addition.